Pervasive Monitoring of Motion and Muscle Activation: Inertial and Mechanomyography Fusion

Richard B. Woodward, *Member, IEEE*, Sandra J. Shefelbine, and Ravi Vaidyanathan, *Member, IEEE*

***Abstract*—Muscle activity and human motion are useful parameters to map the diagnosis, treatment, and rehabilitation of neurological and movement disorders. In laboratory and clinical environments, electromyography and motion capture systems enable the collection of accurate, high-resolution data on human movement and corresponding muscle activity. However, controlled surroundings limit both the length of time and the breadth of activities that can be measured. Features of movement, critical to understanding patient progress, can change during the course of a day and daily activities may not correlate to the limited motions examined in a laboratory. We introduce a system to measure motion and muscle activity simultaneously over the course of a day in an uncontrolled environment with minimal preparation time and ease of implementation that enables daily usage. Our system combines a bespoke inertial measurement unit (IMU) and mechanomyography sensor, which measures the mechanical signal of muscular activity. The IMU can collect data continuously, and transmit wirelessly, for up to 10 h. We describe the hardware design and validation, and outline the data analysis (including data processing and activity classification algorithms) for the sensing system. Furthermore, we present two pilot studies to demonstrate utility of the system, including activity identification in six able-bodied subjects with an accuracy of 98%, and monitoring motion/muscle changes in a subject with cerebral palsy and of a single leg amputee over extended periods (∼5 h). We believe these results provide a foundation for mapping human muscle activity and corresponding motion changes over time, providing a basis for a range of novel rehabilitation therapies.**

***Index Terms*—Heterogeneous sensing, inertial measurement unit (IMU), mechanomyography (MMG), pervasive monitoring.**

Manuscript received October 31, 2016; revised January 31, 2017 and April 28, 2017; accepted May 10, 2017. Date of publication July 17, 2017; date of current version October 13, 2017. Recommended by Technical Editor X. Jing. This work was supported in part by the James Dyson Foundation, and in part by the Engineering and Physical Sciences Research Council under Grant EP/F01869X. *(Corresponding author: Richard B. Woodward.)*

R. B. Woodward and R. Vaidyanathan are with the Department of Mechanical Engineering, Imperial College London, London SW7 2AZ, U.K. (e-mail: rwoodward@northwestern.edu; r.vaidyanathan@imperial.ac.uk).

S. J. Shefelbine is with the Department of Mechanical and Industrial Engineering, Northeastern University, Boston, MA 02115 USA (e-mail: s.shefelbine@neu.edu).

This paper has supplementary downloadable material available at http://ieeexplore.ieee.org.

Color versions of one or more of the figures in this paper are available online at http://ieeexplore.ieee.org.

Digital Object Identifier 10.1109/TMECH.2017.2715163

I. Introduction

MECHATRONIC systems monitoring human activity are now accepted as fundamental components in biophysical analysis, with strong impact in fields such as physiotherapy, motor control, rehabilitation, and sports performance [1]–[5]. Simultaneous measurement of physical movement and muscle activity can identify physiological features indicative of health, neural functionality, and response to rehabilitation or training. Their fusion, however, is normally conducted in laboratory or clinical environments, which restricts the activities that can be tracked as well as the collection time window; pervasive data (collected externally, outside of a laboratory) is not possible. Furthermore, observations in controlled environments do not identify issues that arise while moving naturally in the real world. An unobtrusive, wearable system capable of logging data from motion and muscle activity for extended periods in the field has the potential to significantly impact research and clinical practice in sensory-motor control. Patient activity monitored pervasively would enable improved disease diagnoses, tracking of rehabilitation progress, and the provision of remote therapy [6].

Motion analysis in laboratory settings is typically executed with optical (visual) tracking, which is reliant on cameras and reflective markers attached to the tracked object. Optical systems (e.g., Vicon) have the benefit of high accuracy, but are also costly, nonportable, vulnerable to camera occlusions (due to incorrect camera positioning or other moving objects in the collection space), and rely on equipment mounted away from the subject. A small body of work has attempted to overcome these limitations with wearable vision based systems (e.g., [7]); however, miniature, embedded systems such as inertial measurement units (IMUs) have become a popular option in complementing optical system information, or in situations where optical methods are infeasible [8], [9]. Wearable IMUs surmount issues of portability, occlusion, and price, but at the cost of accuracy.

Today, measurement of muscle activity is performed almost exclusively with surface wet-electrode electromyography (EMG), which measures electrical activity in muscle, typically to assess the initiation or intensity of muscle movement. Surface EMG normally requires single-use electrodes, electrical conductive gel, and preparation such as shaving and abrasion of the skin. These requirements, coupled with the need for a sustained electrical connection for signal quality, can limit prolonged EMG

monitoring. Signal degradation over time and problems associated with skin impedance remain issues to be overcome [10]. Dry EMG electrodes remove the need for conductive gel; however, similar challenges exist due to skin impedance, signal variance due to perspiration, and skin preparation [11]. Recent work has introduced textile-based EMG sensors to surmount issues at the skin-electrode interface [12]. While such approaches hold significant future potential, complementary approaches to the electrical measurement of muscle activity remain an underexplored field.

Mechanomyography (MMG) offers an alternative method to monitor muscle activity. MMG involves measurement of low-frequency (2–200 Hz) vibrations emitted by skeletal muscle during contraction. Its signal reflects the mechanical activity generated by lateral oscillation of muscle fibers [13]. Although MMG is less mature and suffers from a lack of established sensors, capture, and processing practice, it nevertheless offers potential benefits versus EMG such as ease of application, higher signal-to-noise ratio, multiple uses for a single sensor, immunity to changes in skin impedance, and elimination of the need of shaving and conductive gel [14]–[16]. The lack of established systems for MMG capture, however, has significantly limited its scope.

While research on wearable and embedded systems has increased significantly in recent years [17]–[19], only a small body of research has attempted to fuse muscle activity and motion data capture outside laboratory/clinical environments to exploit complementary aspects of each dataset. These efforts, however, have focused principally on EMG, which narrows their collection time and range, leading to potentially unreliable signal quality over a prolonged time [20]–[22]. While these developments offer a wealth of future promise, utility at present has been restricted to laboratory demonstrations in controlled environments. Simultaneous data collection, heterogeneous data fusion, and physiological feature identification are unresolved.

The goal of our research is to develop a multimodal mechatronic sensing system enabling seamless collection of physiological data in any real-world environment. Monitoring in an external environment allows for natural activity, which may be hidden in laboratory settings where activity is controlled. In this investigation, we present the development and integration of new hardware, algorithms, and software leading to a complete zero-preparation, unobtrusive, wearable, motion/muscle activity monitoring system. The system is capable of robust capture, synchronization, and analysis of acoustic muscle activity and physical movement. To our knowledge, it is the first to combine MMG with inertial measurement in a wearable system allowing long-term continuous data capture.

II. Mechatronic Sensor Design and Validation

Our research team has designed and, through iterative prototypes, optimized a new sensor for MMG monitoring. The sensor is packaged with a custom-made IMU we have developed for simultaneous data capture. The IMU/MMG sensing package has been validated in a series of experiments establishing its capacity for accurate muscle and motion data collection.

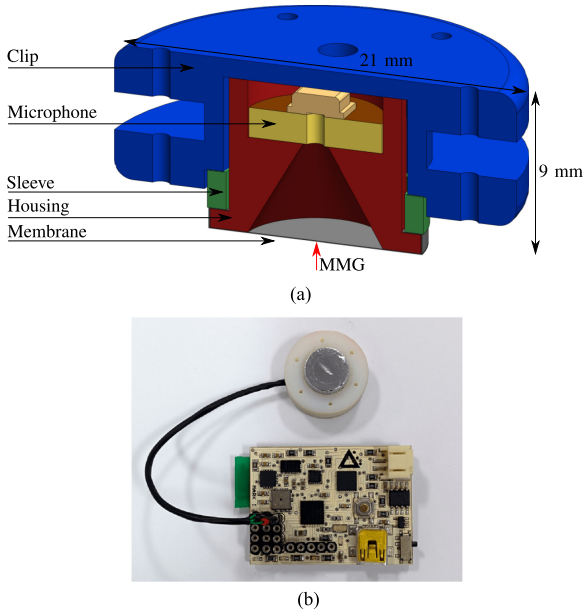

Fig. 1. Hardware used in this study. (a) Rendering of the developed MMG sensor. The device is comprised of a clip/cap (blue) for attachment to clothing and to compress all the parts together, a sleeve (green) to keep the membrane (gray) taut, and the acoustic chamber/housing (red). The electronic board (yellow), which holds the microphone, can also be seen. (b) MMG sensor paired with the Aktiv IMU [27].

A. Sensor Design

1) Mechanomyography: The MMG sensor introduced in this paper consists of a diaphragm covering a sealed chamber dimensioned to capture low-frequency vibrations, adapted from that first presented by Posatskiy and Chau [23]. In our design, a sensor detects pressure change from the base of a sealed chamber. The chamber is covered using a piece of Mylar (aluminum coated with no known allergic risks), and a microphone (Knowles SPU1410LR5H-QB) positioned at the opposite end of the chamber records the pressure change when the membrane is disturbed. When the device is placed on the skin above a superficial muscle, the lateral contractions produce a low-frequency vibration, nominally around 25 Hz with the majority of signal power below 50 Hz, which propagates through the membrane and creates a pressure difference within the chamber [13], [24]–[26]. Following the technical specifications of Posatskiy and Chau, a chamber height and diameter of 5 and 7 mm, respectively, were used, which they report produces maximum gain, reduces the frequency-response fluctuation, and reduces high-frequency distortions. Its conical shape increases signal gain by 6.79 dB/Hz [23].

Fig. 1(a) shows a schematic of the sensor that measures 21 mm $\times$ 9 mm (⌀xH). The Mylar membrane is wrapped around the base of the device and is held in place using a sleeve and friction compression of all the parts fitting together. The clip in Fig. 1(a) (seen in blue) has a number of features to enhance the usability of the device, including a double-level groove, which allows attachment to fabric, and small holes in the top to allow for sewing to clothing. Although thicker than a typical EMG electrode [$\sim$20 mm $\times$ 1.5 mm (⌀xH)], the MMG sensor described

TABLE I
TYPICAL POWER CONSUMPTION OF EACH MAJOR COMPONENT USED IN THE AKTIV IMU AND MMG SENSOR

Component	Model number	Power consumption
Gyroscope	L3G4200D	6.1 mA
Accelerometer	ADXL345	140 μA
Magnetometer	HMC5883L	100 μA
Barometer	BMP085	5 μA
Microcontroller	dsPIC33FJ128GP802	63 mA
Bluetooth	RN41	65 mA
USB battery charger	MAX1811	0.9 mA
USB/UART data chip	FT232RQ	70 μA
MMG microphone	SPU1410LR5H-QB	120 μA

here has a sufficiently low profile, can be used multiple times, and does not hinder movement or range of motion.

2) Inertial Measurement Unit: Our custom made IMU, dubbed the Aktiv [45 mm × 30 mm × 9 mm (L × W × H)], can be seen in Fig. 1(b) next to the MMG sensor. It has a 2000°/s triaxis gyroscope (STMicroelectronics L3G4200D), a ±16 g triaxis accelerometer (Analog Devices ADXL345), a ±8 G triaxis magnetometer (Honeywell HMC5883L), and a −500 to +9000 m (sea level) barometer (Bosch BMP085). The barometer is also capable of monitoring temperature (0.1 °C resolution) that can be used to assist in reducing drift when calculating inertial position. All components were sampled using a 16-bit peripheral interface controller (PIC) microcontroller (Microchip dsPIC33FJ128GP802). Furthermore, the Aktiv contains a bluetooth module (Microchip RN41), universal serial bus (USB) battery charger (Maxim Integrated MAX1811), a micro secure digital (SD) card port, and a USB/universal asynchronous receiver/transmitter (UART) data transmission chip (FTDI Chip FT232RQ). The microcontroller's analog-to-digital converter (ADC) allows sampling from up to four MMG sensors in this application; however, other analog sensors could be used instead. Both inertial and ADC data can be transmitted via bluetooth or USB to a laptop, phone, or tablet, or stored on a removable micro SD card for offline data processing. Data packets are accompanied with a header byte and two checksum bytes at the start and end of the packet, respectively. Header bytes indicate the data type being transmitted (ADC or inertial information), whereas the checksum bytes are used to determine successful transmission and storage. Real-time date and time is possible due to a 32.768 kHz crystal oscillator (ECS Inc., ECX-31B) and can be time stamped to the data before processing. Typical power consumption of each major component can be seen in Table I.

Gyroscope, accelerometer, and magnetometer data are sampled at 50 Hz, barometer at 1 Hz, and ADC data at 1 kHz. The IMU and all connected devices to the ADC are powered by a 1000 mAh lithium-ion battery [50 mm × 33 mm × 6 mm (L × W × H)], which provides around 10 h of battery life on a single charge.

B. MMG Sensor (Hardware) Validation

1) Validation of Frequency Sensitivity: To determine the ability of low-frequency collection using the MMG sensor, an apparatus was constructed to be used with a custom made vibration rig, which oscillates at a fixed frequency. An MMG sensor was sandwiched between a wooden base and a sheet of Plexiglas with the chamber pointing upward. A plastic point was attached to the vibrating rig that tapped the Plexiglas on each oscillation; Fig. 2(a) shows a cross section of the apparatus. The Plexiglas interface was used in order to protect the MMG membrane. The amplitude was set to a peak of 1 V and the frequencies were increased logarithmically from $10^{0.2}$ to $10^{2.4}$ Hz with increments of 0.2.

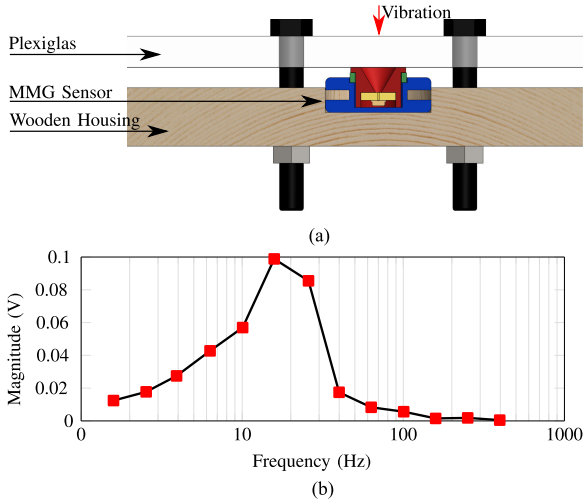

Fig. 2. MMG frequency validation experiment setup. (a) Cross section of apparatus used. (b) Frequency sweep of MMG sensitivity.

A force gauge (Endevco Corp. model 2103-100) was positioned on top of the mass of the rig and was used to validate the MMG sensor. Data were sampled from both the force gauge and MMG for 10 s at each frequency of oscillation at 1 kHz and were each passed through a fast Fourier transform. Accuracy was calculated as the difference between the MMG and force gauge dominant frequencies. To analyze the true response of the sensor, the MMG data were neither filtered nor smoothed.

Results produced from the vibration rig were highly accurate with a low frequency 1.74% (standard deviation (STD) 1.17) when MMG was compared against the outputted force gauge frequencies. The frequency sweep can be seen in Fig. 2(b), which shows a detectable magnitude in the MMG range of interest between 1 and 100 Hz, and a peak magnitude between 10 and 50 Hz, which as mentioned previously contains the majority of MMG signal power.

2) Validation of Isometric Muscle Contraction Data: Physiological comparisons between EMG and MMG for isometric contractions have been well studied in the literature [28]–[30]. To validate our MMG sensor's ability to monitor muscular activity, we performed a validation study where we compared EMG and MMG activity of the extensor carpi radialis longus during isometric extension of the wrist. Both EMG and MMG signals were amplified using an ISO-DAM8A isolated biological amplifier (MMG gain 10×, EMG gain 1000×) and were bandpass filtered between 10 Hz and 1 kHz (analog single pole resistor–capacitor). Both were sampled at 1 kHz using a CED Power1401 data acquisition (DAQ) board.

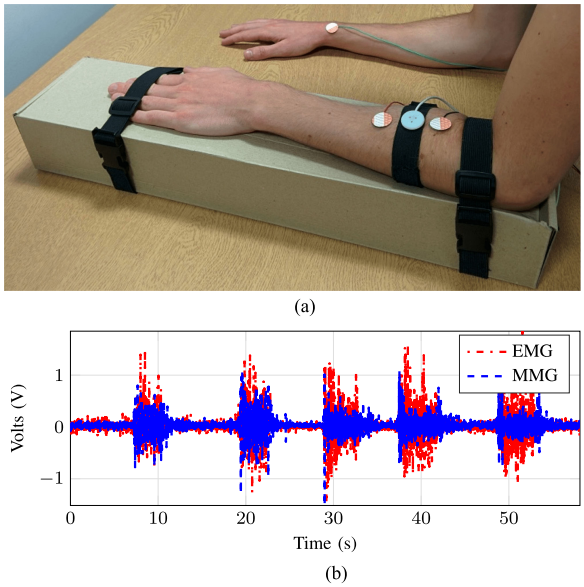

Fig. 3. (a) Isometric contraction experiment setup. (b) Isometric contractions from the extensor carpi radialis longus muscle with EMG (red dot-dashed) and MMG (blue dashed) response.

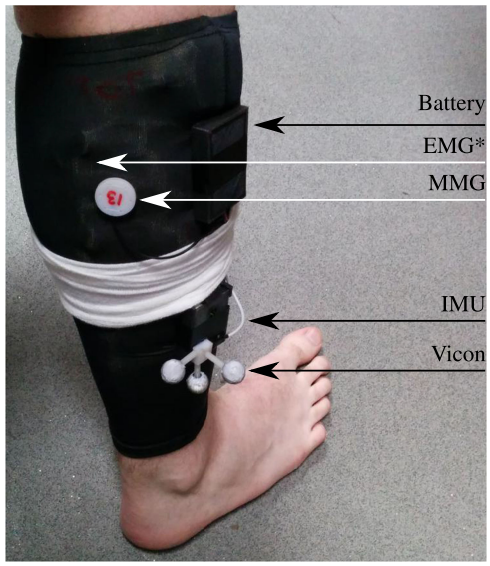

Fig. 4. Image of the calf brace containing IMU, MMG, Vicon, and EMG technologies. The MMG acoustic sensor was positioned atop the gastrocnemius, whereas the EMG electrodes were situated either side the MMG underneath the brace (* not visible).

Contractions were determined during extension of the wrist while monitoring the extensor carpi radialis longus on the subject's left arm with both EMG and MMG [see Fig. 3(a)]. A subject performed an isometric contraction of 100% maximum voluntary contraction by extending their wrist and holding the contraction for approximately 5 s. This was repeated five times with a 5 s break in-between. Contraction responses seen in Fig. 3(b) show five repetitions of a sustained isometric contraction from both EMG (red dot-dashed) and MMG (blue dashed).

Both EMG and MMG signals were smoothed using a five-point moving average algorithm and rectified. If $\widetilde{m}$ is the EMG or MMG output, the time window of muscle activation between onset time $[a]$ and offset time $[b]$ can be found with (1). Onset and offset of the muscle contractions for EMG and MMG signals were detected by noting when the average power of a 500 ms nonoverlapping muscle activation signal segment exceeded and then fell below an empirically determined threshold (2). A suitable threshold of 0.135 V was found experimentally as a point greater than both EMG and MMG resting voltages and around 50% lower than their largest contraction magnitude

$$E_{a,b} > T, \text{ where } E_{a,b} = \{E_a, E_{a+1}, \ldots, E_b\} \tag{1}$$

$$E_j = \frac{1}{N} \sum_{k=j-N+1}^{j} m_k^2. \tag{2}$$

The parameters T and N in (1) and (2) are the detection threshold and the duration of the energy window, respectively. Thus, when the average power over a window (N) of the signal rises and maintains a value above a designated threshold (T), the time indices of the vector $\widetilde{m}$ at E_a and E_b will give the onset and offset time of muscle activation. Comparison of isometric muscle monitoring technologies showed that MMG signal onset preceded EMG with a difference of 41 $\pm$ 181 ms; MMG offset occurred after EMG at 204 $\pm$ 223 ms.

C. Validation of Dynamic Motion and Muscle Contraction Data

1) Experimental Setup: To validate the sensor's ability to collect motion and muscle data concurrently, a ten camera Vicon system and a Myon EMG system were used at the same time as one of our Aktiv IMUs and MMG sensors in a local gait analysis laboratory. Fig. 4 shows all devices attached to a calf sleeve. A triple-quiver marker was placed on top of the IMU, which was tracked by the Vicon cameras, whereas the EMG and MMG sensors were placed on the lateral head of the gastrocnemius. The Vicon system sampled both the optical data and controlled the sampling of the EMG data (transmitted over a propriety wireless protocol). The Aktiv IMU concurrently collected the inertial and MMG information and transmitted the data to a laptop computer via bluetooth. The laptop computer was connected to the external trigger of the Vicon system via a National Instruments DAQ (USB-6210) and used MATLAB to synchronously start and stop data collection from all technologies simultaneously. Vicon was sampled at 100 Hz, IMU at 50 Hz, and EMG and MMG at 1 kHz. In order to compare Vicon and IMU data, Vicon was down sampled to 50 Hz to match the IMU.

Muscle activity from the gastrocnemius muscle and motion of the lower leg were recorded as the subject walked and climbed stairs in the laboratory. Two subjects, both male, performed three tasks: walking, ascending stairs, and descending stairs, for five trials of each. Out of the five trials for each task, the four with fewest Vicon marker drops were taken and analyzed.

2) Data Analysis: Vicon results were output as positional data and a single X (internal/external rotation), Y (abduction/adduction), and Z (flexion/extension) coordinate was determined by finding the center position of the triple-quiver marker set. Positional data were differentiated twice to obtain velocity and acceleration. All data were resized to include only motion

within the center of the laboratory and then smoothed using a three-point moving average algorithm. The magnitude (Euclidian norm) of the accelerations from the Aktiv was calculated using (3), where n is the number of samples and d is the dimension (three, representing each respective accelerometer plane) of each sample

$$|a| = \sum_{i=1}^{n} \left(\sum_{j=1}^{d} (x_{ij})^2 \right)^{\frac{1}{2}}. \tag{3}$$

Stationary periods were determined whenever the magnitude dropped below 66% of the maximum. These points were used as ground truths to correct results and remove drift from the raw data. Using a gradient descent attitude and heading reference system developed by Madgwick *et al.* the inertial raw data were converted to quaternions that allowed the results to be aligned to the earth's coordinate frame, which determined the global accelerations [31]–[33]. Gravity was removed during the calculations to avoid a biased coordinate frame, while information from the accelerometer, gyroscope, and magnetometer were all used in this algorithm. Velocity and position were obtained by integrating. The IMU was turned on 30 min prior to testing to stabilize temperature fluctuations to reduce drift in the velocity and position calculations. The temperature was monitored by the barometer (sampling at 1 Hz). The accelerations, velocities, and positions of the Vicon and IMU data were compared using root mean square error (RMSE) differences to determine accuracy. The RMSE was determined by (4), where N is the total number of data samples, VD is the Vicon accelerations/velocity/position, and ID is the same for the IMU. This value was converted into a percentage error for ease of analysis. All data were processed in MATLAB

$$\text{RMSE} = \sqrt{\frac{1}{N} \sum_{n=1}^{N} |\text{VD} - \text{ID}|^2}. \tag{4}$$

In order to reduce artifacts in MMG data, the accelerometer data were normalized between one and zero and resampled to 1 kHz to match the MMG sampling rate. The MMG data were filtered using a digital first-order bandpass Butterworth filter between 10 and 100 Hz, and then divided by the magnitude of the acceleration (5), where n is the current data point, NMA is the normalized magnitude of the accelerometer, and MMGS is the smoothed MMG signal. At time intervals with large magnitude accelerations (such as impact), the MMG data were significantly reduced. However, when accelerations were small, the MMG activity changed marginally. In total, 20 strides from both subjects across these tests were used and analyzed using the same energy thresholding technique (2) discussed previously to determine onset and offset differences between MMG and EMG

$$\text{MMGS}_n = \frac{\text{MMG}_n}{\text{NMA}_n}. \tag{5}$$

3) Validation Results: Analysis of the results produced from simultaneous Vicon and IMU validation showed a high accuracy across each plane and activity. Table II shows the results of three activities [level walking (LW), stair ascend (SA), and stair descend (SD)] for all three of their planes (X, Y, and Z), and all three dynamic types (acceleration, velocity, and position). Integration errors caused less accuracy in position compared to velocity and acceleration. Results were better in the planes exposed to more motion.

TABLE II
RMSE RESULTS FOR VALIDATION OF MOTION DATA

%	A_X	A_Y	A_Z	V_X	V_Y	V_Z	P_X	P_Y	P_Z
LW	83.1	**90.8**	**91.3**	**94.0**	**91.9**	**93.9**	67.8	81.8	89.5
SA	**95.0**	**95.8**	**94.7**	89.3	88.9	**90.8**	65.7	82.9	**90.6**
SD	87.4	**91.5**	**93.9**	**90.4**	**91.2**	82.6	76.9	87.7	88.2

An accuracy of 100% indicates identical results between Vicon and IMU results. Results above 90% have been made bold. LW = level walking; SA = stairs ascend; SD = stairs descend. A, V, P = accelerations, velocities, and positions for X, Y, and Z planes.

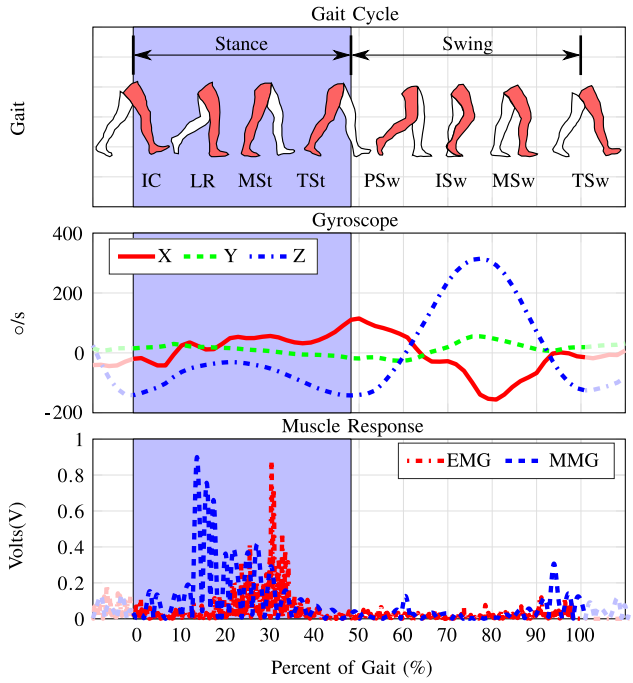

Fig. 5. Analysis of motion and muscle response during one gait cycle. Top—gait cycle; the stance phase consists of initial contact (IC), loading response (LR), mid stance (MSt), terminal stance (TSt), and preswing (PSw), whereas the swing phase consists of initial swing (ISw), midswing (MSw), and terminal swing (TSw). Middle—motion; gyroscopic data. Bottom—muscle response; EMG (red dot-dashed) and MMG (blue dashed). The blue shaded background represents the stance phase during gait.

Analysis of muscular activity showed that MMG contraction duration (383 ± 188 ms) exceeded that of EMG (201 ± 106 ms), and in most cases MMG began before EMG contraction response by 107 ± 212 ms. Peak EMG and MMG signals were in the stance stage of gait, which was expected due to the majority of muscular activity from the gastrocnemius being produced during plantar flexion of the ankle (see Fig. 5) [34].

III. PHYSICAL ACTIVITY CASE STUDIES

We have implemented the system in two physical activity case studies to illustrate its utility for biophysical analysis. Each

draws from its validation experiments and data fusion architecture. The first illustrates the identification and classification of key activities in real-world gait using both sensing muscle and motion modalities. The second outlines the implementation of the system for pervasive monitoring in subjects with irregular gait [a cerebral palsy (CP) subject and a unilateral amputee] in natural environments for extended periods during their activities of daily living. All studies were approved by the Imperial College Research Ethics Committee and written consent was obtained from all subjects involved.

A. Case Study I: Activity Classification Through Parallel Muscle and Motion Tracking

Six able-bodied subjects were recruited, one female and five male, aged between 25 and 31 (STD 2.34) and a height of 165–185 cm (STD 7.34), to perform a number of differing activities (standing, lying, walking, running, ascending/descending stairs, ascending/descending within an elevator) for a period of time during an experiment to validate the accuracy of a novel activity classification algorithm. Briefly, this algorithm splits data into windowed segments that were classified into a broad cluster group (stationary standing, lying, and elevator; dynamic walking and running; or dynamic-altitude stairs) and then refined into specific activities. A detailed formulation of this protocol is presented in the appendix.

The subjects, all with typical gait, were selected on their differing height, as opposed to sex, weight, or ability. Height influences stride length and cadence, which were a key element in classifying walking from running in this algorithm. Each subject performed two trials in which they took a pseudorandom walk lasting 10 min involving multiple activities from the list above, while given a different set of activities to perform. Subjects were not asked to perform their tasks in a particular order, length of time per activity, nor instructed in how to perform the task; they were only asked to perform their given tasks at least once during their trials. The IMU is situated on the lateral side of their right leg and the MMG sensor on the lateral head of the gastrocnemius (similar to Fig. 4). A push button was used, which the subject pressed before changing to a different activity, in order to validate the data collected against a ground truth.

In order to determine the robustness of the algorithm, each subject was asked to perform differing activities where some do not perform any tasks from the dynamic, stationary, or dynamic-altitude-based groups. Some subjects were asked to avoid tasks such as ascending/descending stairs, in order to remove any classification from the dynamic-altitude-based group, whereas others were asked to only perform stationary tasks, to remove both dynamic and dynamic-altitude tasks. An investigator accompanied each subject on their trials to record what activity they performed, and at what time, so that these data could be compared against the activity determined by the algorithm. Accuracy was determined by validating each window activity against its recorded actual activity. The subjects pressed a button each time they changed activities that were collected alongside inertial and MMG data. The button presses created known points of activity change, which were used to further assist in validation. In order to validate the improvement through MMG inclusion in the algorithm, the data were processed twice. Once with both motion and muscle information and another with the muscle data component removed. The accuracy of the algorithm with MMG was compared against that without MMG, in order to determine its importance in the classification of activities. Data processed with MMG and without MMG was passed through a paired *t*-test to determine significance. The algorithm was tested on pervasive data in which activities were manually recorded.

TABLE III
RESULTS OF ACTIVITY CLASSIFICATION WITHOUT AND WITH MMG

Subject	Activities	Missing Group	% w/o MMG	% w/ MMG
1	S, LW, SD, EA	None	99.2	99.2
2	S, LW, SA, ED	None	96.3	96.3
3	S, LW, SA, SD	None	97.5	97.5
4	S, LW, EA, ED	Dynamic altitude	98.3	98.3
5	S, LW, R	Dynamic altitude	89.2	99.3
6	S, L	Dynamic, Dynamic altitude	100.0	100.0
Avg.			96.8	98.4

S = standing; L = lying; LW = level walking; R = running; SD = stairs descend; SA = stairs ascend; ED = elevator descend; EA = elevator ascend.

The overall algorithm accuracy, by taking the mean of accuracy across all subjects and trials, was found to be 97% without MMG, and 98% with MMG (see Table III).

B. Case Study II: Pervasive Monitoring of Motion and Muscle Activity in Patients With Atypical Gait

Three subjects, asymptomatic (control), hemiplegic CP, and unilateral transtibial (below the knee) amputee, were monitored during their normal daily routine. Muscle signal amplitudes from an MMG sensor on the gastrocnemius muscle were analyzed and any change reported while movement patterns were monitored for change using an Aktiv IMU.

The IMU was mounted on the lateral side of the right leg, and the MMG sensor situated on the lateral head of the gastrocnemius. The right leg was the amputees nonamputated leg, whereas the right leg of the CP subject was his affected side, therefore each subject (including asymptomatic) wore the brace on their right leg. A similar brace, as seen in Fig. 4, was used in this study including the IMU and MMG technologies.

On a typical day, each subject put the sensor on when they woke up and collected approximately 5 h of data. The brace required no special training other than some brief instructions on where the MMG sensor had to be placed over the gastrocnemius. As everything was sewn in place, the correct positioning of the MMG sensor meant that the IMU was also positioned correctly. Data were saved to the device's SD card and all processing was performed offline. The same sampling rates and processing methods were used as presented in Section III-A.

The "walking" activity data were used and analyzed in determining activity change over time; the other activities were not further analyzed within this study, however, could be used in future applications. Following from the classification of walking data, individual strides were identified using a thresholding method that looked for peaks in the gyroscope Z plane

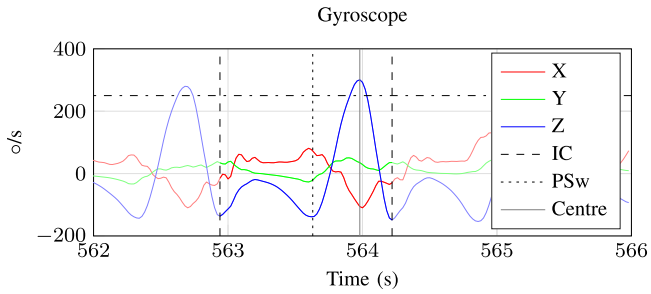

Fig. 6. Figure displaying the process taken for individual stride segmentation from gyroscopic data of the lower leg. The black horizontal line shows the threshold in which gyroscope data from the *Z* plane (which represents gait swing) had to exceed. The gray vertical line represents a center peak, which exceeds this threshold. Data between IC and IC represent one stride. These data were taken from the asymptomatic gait subject.

TABLE IV
AVERAGE DURATION (PERCENT OF TRIAL) OF EACH OF THE CLASSIFIED ACTIVITIES

Subject	Standing/Sitting	Walking	Noise/Other
Asymptomatic	75%	16%	9%
Amputee	46%	45%	9%
CP	54%	44%	2%

Only walking, standing/sitting, and noise/other activities had a percentage above 1%. Activities below 1% are not shown here.

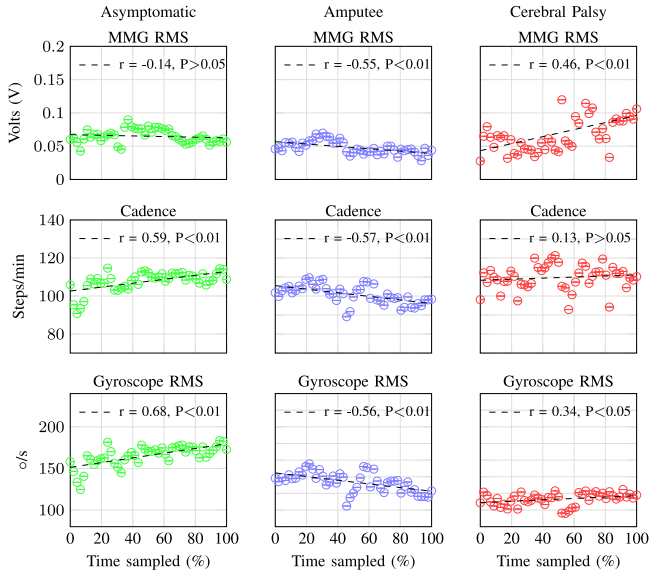

Fig. 7. Results for progressive changes in the gastrocnemius between typical and atypical gait. Each plot has linear regression line plotted as well as their corresponding Pearson's correlation coefficient (*r*) and *P* values.

(>250°/s), which represented the flexion/extension of gait (see Fig. 6). Recognizing the repeatable gyroscopic pattern for each stride, the preswing (PSw) phase of gait was identified as the first minimum prior to the center point, whereas working further backward to the next minimum was recognized as the initial contact (IC) phase of gait. Working forward from the center point, the first minimum was the IC of the next stride. The data between IC and IC represent one stride.

To determine change in motion over time, the gyroscopic magnitude (3) from each stride was determined and the amplitude (RMS) of that signal was calculated. Furthermore, the cadence of each stride was determined by taking the stride duration and calculating the step duration and then estimating the steps per minute. Muscle activity was denoised of vibration artifact (5) and the RMS of the MMG signal was calculated from the flat foot stage of each stride (between IC and PSw in Fig. 6).

In order to determine changes in muscle activity or motion over time, linear regression analysis was performed on the MMG RMS, cadence, and gyroscope magnitude against time. For each, the Pearson's correlation coefficient (*r*) was calculated, along with significance value (*P*), and percentage change over time, from the start to finish of the total time sampled.

Table IV shows the average duration (percent of trial based on the time of trial duration per subject) of the activities performed by each subject group during their collection trial, whereas Fig. 7 displays the motion and muscular response change over time. The asymptomatic subject saw a nonsignificant decline in MMG RMS (−7%) with a significant increase in both cadence (10%) and gyroscope RMS (19%). The subject reported no discomfort, fatigue, or tiredness at the end of the trial; however, they were unaware of any voluntary changes in their gait over the trial either. The amputee subject's motion and muscle parameters all significantly decreased during the collection period: MMG RMS by −31%, cadence by −9%, and gyroscope RMS by −15%. The subject reported tiredness in their calf muscles following the trials, as they normally feel on active days. The CP subject saw significant increases in MMG RMS (122%) and gyroscope RMS (8%); however, a nonsignificant change was seen in cadence (3%). The subject reported a feeling of muscle loosening and a decline in joint stiffness over the course of the day. Average cadence speeds were found to be 108 ± 5 steps/min, 102 ± 4 steps/min, and 107 ± 2 steps/min for asymptomatic, amputee, and CP subjects, respectively. Likewise, average gyroscope RMS results were found to be 166 ± 20°/s, 133 ± 13°/s, and 113 ± 4°/s, in asymptomatic, amputee, and CP subjects, respectively.

IV. DISCUSSION

Previous studies have developed MMG sensors using accelerometers, microphones, piezoelectric transducers, laser distance sensors (LDS), and hydrophones [35]–[40]. In this paper, we used microphones due to their accurate results and higher rejection of motion noise compared to other methods, specifically accelerometers [41]. Other methods, such as LDS and hydrophones, are impractical for this paper, due to size/cost and lack of pervasiveness.

IMUs are widely used in aeronautic applications [42], [43], but have more recently been applied to human motion analysis [44]–[46], and are available in a range of forms, such as complete commercial packages (Xsens, x-IMU, MotionNode), breakout boards and prototype circuits, and all-in-one integrated circuit

chips. Despite the wide availability in the market, limitations such as lack of functionality, which allows simultaneous MMG collection, or practicality (size, weight, battery life), required the development of a custom made IMU. The Aktiv was designed specifically to be light, low cost, low power, and wireless. Its built-in auxiliary port, which allows fast sampling from up to four analog sensors, is what makes this device novel as this feature is scarcely found in current commercial IMUs and is a requirement for simultaneous inertial/MMG collection. Furthermore, IMUs that do feature an on-board auxiliary port for concurrent sensor acquisition have insufficient sampling rates (<512 Hz), whereas the Aktiv can sample up to 1 kHz, which is much better suited for EMG and MMG collection. Parts, manufacturing, and assembly of the Aktiv IMU and MMG sensors come to a cost of $250 and $15 USD per sensor, respectively. This compares very favorably with EMG, where wireless systems can cost in excess of $3000 [47], and optical systems, which exceed this by an order of magnitude. The technology presented here was designed with fast utilization in mind to reduce time taken in donning and doffing, calibration, or marker/electrode placement needed in other technologies; it is entirely unobtrusive, immune to any occlusion inhibiting optical data collection, robust to sweat or other interference, and leaves the subject free to execute any other activity while wearing/using the system.

Our study validating the Aktiv IMU against Vicon, the gold standard of human motion monitoring, reported a close comparison in accuracy for determining acceleration, velocity, and position. The calculation of absolute position from an IMU can result in drift, due to the integration stages of conversion, and therefore IMUs are infrequently used for determining position.

Frequency sensitivity and isometric muscle contraction validation showed a suitable response across the MMG frequencies of interest and suggest our designed sensor can be suitably used in MMG applications or applications where EMG is infeasible. However, an earlier and later MMG onset and offset was seen when comparing isometric contractions to EMG in our "Validation of Isometric Muscle Contraction Data" study (see Section II-B2). This is likely due to skin artifacts produced by small movements of the sensor during contraction. Likewise, dynamic contractions and the resulting MMG data are susceptible to motion artifacts, along with oscillation noise caused during IC (heel strike) and initial swing (ISw) (toe off) when monitoring lower limb muscles during gait. Our research has shown how noise, such as impact vibration and motion, can be filtered from the MMG data using the IMU accelerometer data as a guide to where impacts occurred. This method works to reduce motion artifacts, which occur outside of the contraction period of the muscle of interest. Fig. 8 shows this filtering process, including gyroscopic data, accelerometer data with calculated magnitude, unprocessed (raw) MMG data, filtered MMG data, and filtered and processed MMG (top to bottom, respectively). It can be seen that in the unprocessed and filtered MMG plots, it is difficult to determine contraction periods due to the vibration artifacts (IC is highlighted with a red background). The processed MMG data have been filtered and smoothed, and motion and shock artifacts have been removed. gastrocnemius muscle activation occurs at 10% of the gait cycle [end of loading response (LR)],

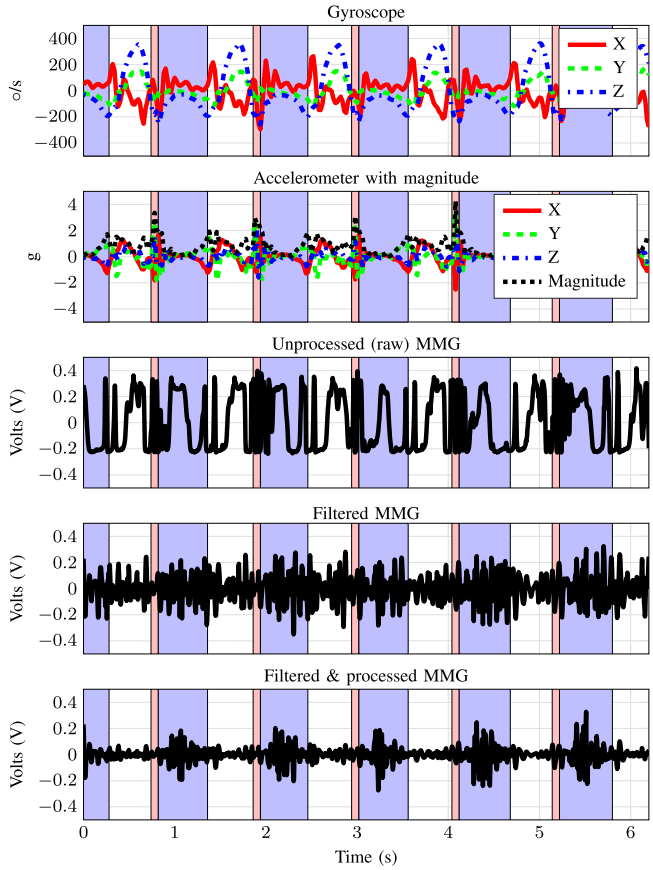

Fig. 8. Stages of MMG signal denoising. Blue shaded backgrounds represent time periods of flat foot stance during gait, whereas red-shaded backgrounds represent heel strike during gait.

with a peak at 40% [mid terminal stance (TSt)], and an offset at 50% (end of TSt) [34]; therefore, due to the expected contraction periods of the gastrocnemius occurring during the stance stage of gait, this method works well in filtering disturbances. A comparison between the top plot (gyroscope data) and the bottom plot (processed MMG) in Fig. 8 shows that the stance stages of gait, highlighted with a blue background, coincide with muscular contraction periods. This method is believed to also work with other muscles, provided their contraction period is not during a high motion moment, such as heel strike or toe off. This limits the method to a handful of muscles, but not necessarily just the gastrocnemius.

Discrepancies between EMG and MMG contraction times, seen in Fig. 5, are believed to be due to motion artifacts produced at the onset and offset of contraction. Although the denoise process reduces disturbances produced during high acceleration point of gait, large onset/offset peaks in MMG data will be minimized, but not completely removed. This is an issue with all MMG measurement. While parallel inertial measurement offers some mitigation, MMG remains more vulnerable to noise and motion/shock artifacts when compared against EMG. There are (potentially complimentary) pros and cons to each measure, which will depend significantly on the collection environment.

Results seen in our first case study (see Section III-A) showed a high accuracy in classification between nine com-

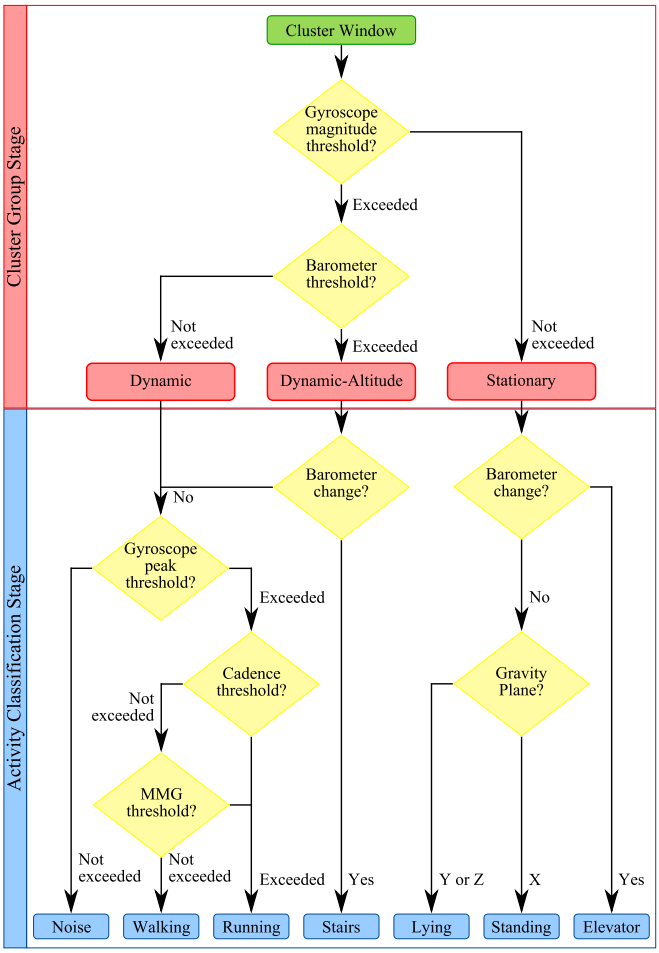

Fig. 9. Two-part *a priori* activity classification flow chart.

monly performed activities. This model was based on previous work, which used multiple IMUs and single accelerometers to determine multiple activities [48], [49]; however, the method presented here was unique in which the model (A) was uncontrolled and unsupervised with no precollection data labeling for activities required and (B) concurrently used muscular activity. The results between subject five's trials were significantly different ($P < 0.05$) in comparison of classification with and without MMG data components (see Table III). All other subject comparisons were not significantly different. This was expected due to subject 5 being the only participant who performed a running task, of which the MMG data assisted in classifying (see Fig. 9). During the start of a running task, it took a number of strides before an accurate cadence could be calculated in order to classify the running activity. Without MMG, the algorithm recognized multiple windows at the beginning and end of a running task, when the subject was speeding up and slowing down, as walking. The inclusion of MMG data allowed for an additional thresholding method, which would recognize muscle activity high enough to be determined as running, before a running cadence value could be estimated. Although the average accuracy of subject 5's trials was high (89%) without MMG data, it was significantly lower than the calculation with MMG (99%). MMG inclusion would produce a larger global margin of improvement in applications where running is more abundant.

Results seen in our second case study (see Section III-B) showed that each subject spent the majority of their collection time standing/sitting; however, both the amputee and CP subjects were active (walking) more than the asymptomatic subject (see Table IV). Due to the IMU being placed on the lower leg, there is no discernible way to classify between standing and sitting; however, both activities are stationary and the current classification methods are sufficient for this task. Cadences among all three groups were unexpectedly similar, with each within the normal cadence speed, matching previously reported average cadence speeds of 90–130 steps/min [50], [51]. Although cadence was similar between groups, the gyroscope RMS results showed higher magnitudes in the asymptomatic group as opposed to amputee and CP results. The decrease in gyroscope RMS from asymptomatic to amputee to CP results is believed to be due to the amputee's compensation of its prosthesis, and the CP hemiplegic spasticity, both of which limit their gait, respectively.

MMG results across CP and amputee subjects showed a significant change over time as well as a moderate linear correlation, whereas the asymptomatic subject showed a nonsignificant change. The much higher percentage of change seen in the CP MMG results suggests their observation of muscle loosening over the course of a day occurs much faster and was much more prominent than the amputee's muscle tiring due to overcompensation. A poor linear correlation in the asymptomatic subject's MMG data suggests no change in muscular activity.

V. Conclusion

The goal of this investigation was to develop and demonstrate the utility of a new concept for human biophysical analysis. While extensive research has been performed in motion and muscle recording, nearly all existing systems have limited scope outside controlled environments due to challenges associated with EMG (electrical) collection of muscle activity, the lack of hardware with the capacity to fuse motion and muscle activity data simultaneously, and the lack of heterogeneous feature extraction algorithms identifying biophysical parameters from data with multiple sources.

We introduce the first system we are aware of addressing all these issues. We have developed, validated, and demonstrated use of a novel MMG and motion analysis sensor for pervasive sensing. This paper has concluded that our custom MMG and IMU sensors are capable of measuring motion and muscle activity during simple motions to a high accuracy when compared against the current gold standard. We have demonstrated that an algorithm can classify human activity into nine activities using an unsupervised algorithm. Finally, the monitoring of progressive changes over time in subjects with atypical gait has also been achieved, showing significant change ($P < 0.01$) in muscular activity.

Future research involves identification of key physiological markers to correlate movement with neurological function or dysfunction in rehabilitation, investigation into optimal filtering

methods for MMG, design of new robotic interfaces for assistive technology and artificial limbs, and home monitoring for conditions such as stroke and Parkinson's disease. Commercial applications being pursued based on this research include interfaces for peripheral device control and clinical monitoring [52].

APPENDIX

We have developed an algorithm to fuse heterogeneous inertial (movement) measurement and MMG muscle activity data to classify a number of commonly performed physical activities. We present the algorithm in the context of gait feature classification; however, the algorithm architecture may be implemented to extract any set of desired features based on simultaneous collection of movement and muscle activity data over extended periods of time.

When implemented for gait feature classification, a total of nine activities were targeted for classification, including walking, running, standing/sitting, lying, ascending/descending stairs, ascending/descending in an elevator, and "other," which contained unprocessed activities and noise. All inertial data (accelerometer, gyroscope, magnetometer, and barometer) were smoothed using a moving average seen in (6) where ys_n is the smoothed value for the nth data point, N is the number of neighboring data points on either side of ys_n, and $2N+1$ is the span, which in this case N is equal to 15 data points

$$ys_n = \frac{1}{2N+1}\left[\sum_{i=1}^{N+1} y_{n+N+1-i}\right]. \tag{6}$$

After smoothing, data from each sensor type were windowed in order to be processed by the algorithm. The inertial window size was set to 200 samples (4 s of data at 50 Hz), which can be easily resized to obtain the same window size for the other sensors sampled at a different rate: a four-sample window for the barometer at 1 Hz, and a 4000-sample window for the MMG at 1 kHz. The data were resized into windows of 4 s with a 50% overlap and four features [mean, standard deviation, power, and covariance (7)] were determined from each of the three axes of the accelerometer (*X*, *Y*, and *Z*) resulting in 12 parameters per window, where n is the current data point, N is the total number of data points in the window, i.e., 200, y is the dataset of one axis, μ is the mean, σ is the standard deviation, and a and b correspond to one of the three accelerometer axes (*X*, *Y*, or *Z*)

$$\begin{aligned}
\mu &= \frac{1}{N}\sum_{n=1}^{N} y_n \\
\sigma &= \sqrt{\frac{1}{N-1}\sum_{n=1}^{N}(y_n-\mu)^2} \\
\text{power} &= \sum_{n=1}^{N}\frac{y_n^2}{N} \\
\text{COV}(a,b) &= \sum_{n=1}^{N}\frac{(a_n-\mu_a)(b_n-\mu_b)}{N}.
\end{aligned} \tag{7}$$

A *K*-means clustering algorithm using a squared Euclidean distance method was used to cluster windowed data into one of three clusters based on the parameter matrix created from the four features above. This algorithm processes the data in two stages: a gross group clustering stage where each window was split into one of three groups; stationary activities (standing, lying, and elevator), dynamic (walking, running, and noise), and dynamic altitude (stairs), and a second activity classification stage where windows from each cluster group were further classified into one of nine activities. The objective function of the *K*-means algorithm is seen in the following equation:

$$J = \sum_{n=1}^{N}\sum_{k=1}^{K} r_{nk}||y_n - c_k||^2 \tag{8}$$

where again y, n, and N are the dataset, current data point, and total number of data points, respectively, K is the number of clusters, i.e., three, k is the current cluster, c is the centroid of the cluster, and r_{nk} is the binary indicator variable (where r_{nk} is equal to one if a data point belongs to cluster k, otherwise zero). In order to predict data points belonging to one of the three cluster groups, the values of r_{nk} and c_k had to be found in order to minimize J. Initial values of c_k are randomly determined, then the two stage process of calculating r_{nk} and c_k were repeated until results converge. As different initial cluster centroids can produce slightly differing results, the algorithm was replicated five times with a new set of initial cluster centroid positions for more accurate results.

1) Centroids of the clusters were initialized with random values.
2) Each data point was attributed to the closest cluster using (9).
3) The position of each cluster is re-evaluated so that it corresponds with the mean of all data points belonging to that cluster using (10).
4) Steps 2 and 3 are repeated until results converge

$$r_{nk} = \begin{cases} 1 & \text{if } k = \text{argmin}_j ||y_n - c_j||^2 \\ 0 & \text{otherwise} \end{cases} \tag{9}$$

$$c_k = \frac{\Sigma_n\, r_{nk}\, y_n}{\Sigma_n\, r_{nk}}. \tag{10}$$

With each window placed within one of three clusters, it was still unknown what group (stationary, dynamic, or dynamic altitude) each cluster belongs to. The average gyroscopic magnitude and barometer gradient were determined from each window of data belonging to each of the three unknown clusters and the cluster average was used to determine which group they belong to. The stationary group was defined by detecting a gyroscopic magnitude below a threshold of 50°/s, the dynamic group determines if the same gyroscopic magnitude data exceeds the same threshold and the barometer gradient was below a threshold of 0.1 ms, and finally the dynamic-altitude group was defined by exceeding both the gyroscopic magnitude threshold and barometer gradient threshold (Fig. 9—Cluster Group Stage). If there are no activities from one of the cluster groups, for example, no stair climbing, no dynamic-altitude group was detected, and the

other cluster groups may have multiple clusters belonging to them. The threshold values used were determined by trial and error prior to this study and were found to sufficiently characterize activities for all subjects tested. These values were not redetermined for each subject and therefore this algorithm still accomplishes an unsupervised methodology.

The second stage of the algorithm processed each window within a cluster group to classify the individual activities by using information from all sensors available and exploiting unique attributes from each of the nine activities (Fig. 9—Activity Classification Stage). MMG data were denoised of vibration artifact as described in Section II-C2. The elevator and stairs activities were further split into two each (ascending/descending) by determining the direction of barometer pressure change.

Acknowledgment

The authors would like to thank all the subjects involved in this study, as well as the Biodynamic Laboratory at Charing Cross Hospital where many of the validation tests were performed.

References

[1] R. T. Lauer, B. T. Smith, and R. R. Betz, "Application of a neuro-fuzzy network for gait event detection using electromyography in the child with cerebral palsy," *IEEE Trans. Biomed. Eng.*, vol. 52, no. 9, pp. 1532–1540, Sep. 2005.

[2] J. W. Youdas *et al.*, "Surface electromyographic activation patterns and elbow joint motion during a pull-up, chin-up, or perfect-pullup rotational exercise," *J. Strength Condition. Res.*, vol. 24, no. 12, pp. 3404–3414, 2010.

[3] G. Shan, "Biomechanical evaluation of bike power saver," *Appl. Ergonom.*, vol. 39, no. 1, pp. 37–45, Jan. 2008.

[4] N. Abaid *et al.*, "Gait detection in children with and without hemiplegia using single-axis wearable gyroscopes," *PLoS ONE*, vol. 8, no. 9, 2013, Art. no. e73152.

[5] J. H. M. Bergmann *et al.*, "Exploring the use of sensors to measure behavioral interactions: An experimental evaluation of using hand trajectories," *PLoS ONE*, vol. 9, no. 2, 2014, Art. no. e88080.

[6] Y. Liang *et al.*, "Energy-efficient motion related activity recognition on mobile devices for pervasive healthcare," *Mobile Netw. Appl.*, vol. 19, no. 3, pp. 303–317, 2014.

[7] K. D. Nguyen, I. M. Chen, Z. Luo, S. H. Yeo, and H. B. L. Duh, "A wearable sensing system for tracking and monitoring of functional arm movement," *IEEE/ASME Trans. Mechatronics*, vol. 16, no. 2, pp. 213–220, Apr. 2011.

[8] H. Fourati, N. Manamanni, L. Afilal, and Y. Handrich, "Complementary observer for body segments motion capturing by inertial and magnetic sensors," *IEEE/ASME Trans. Mechatronics*, vol. 19, no. 1, pp. 149–157, Feb. 2014.

[9] Y. Zhang, K. Chen, J. Yi, T. Liu, and Q. Pan, "Whole-body pose estimation in human bicycle riding using a small set of wearable sensors," *IEEE/ASME Trans. Mechatronics*, vol. 21, no. 1, pp. 163–174, Feb. 2016.

[10] C. Gavriel and A. A. Faisal, "A comparison of day-long recording stability and muscle force prediction between BSN-based mechanomyography and electromyography," in *Proc. 2014 11th Int. Conf. Wearable Implantable Body Sensor Netw.*, Jun. 2014, pp. 69–74.

[11] P. Laferriere, E. D. Lemaire, and A. D. C. Chan, "Surface electromyographic signals using dry electrodes," *IEEE Trans. Instrum. Meas.*, vol. 60, no. 10, pp. 3259–3268, Oct. 2011.

[12] A. Shafti, R. B. R. Manero, A. Borg, K. Althoefer, and M. Howard, "Embroidered electromyography: A systematic design guide," in *IEEE Trans. Neural Syst. Rehabil. Eng.*, vol. PP, no. 99, pp. 1–1.

[13] M. J. Stokes and P. A. Dalton, "Acoustic myography for investigating human skeletal muscle fatigue," *J. Appl. Physiol.*, vol. 71, no. 4, pp. 1422–1426, Oct. 1991.

[14] H.-B. Xie, Y.-P. Zheng, and J.-Y. Guo, "Classification of the mechanomyogram signal using a wavelet packet transform and singular value decomposition for multifunction prosthesis control," *Physiol. Meas.*, vol. 30, no. 5, pp. 441–457, 2009.

[15] D. T. Barry, S. R. Geiringer, and R. D. Ball, "Acoustic myography: A noninvasive monitor of motor unit fatigue," *Muscle Nerve*, vol. 8, no. 3, pp. 189–194, 1985.

[16] M. J. Stokes, "Acoustic myography: Applications and considerations in measuring muscle performance," *Isokinetics Exercise Sci.*, vol. 3, no. 1, pp. 4–15, 1993.

[17] A. I. Adiba, N. Tanaka, and J. Miyake, "An adjustable gaze tracking system and its application for automatic discrimination of interest objects," *IEEE/ASME Trans. Mechatronics*, vol. 21, no. 2, pp. 973–979, Apr. 2016.

[18] G. Chelius *et al.*, "A wearable sensor network for gait analysis: A 6-day experiment of running through the desert," *IEEE/ASME Trans. Mechatronics*, vol. 16, no. 5, pp. 878–883, Oct. 2011.

[19] F. Jasni, N. A. Hamzaid, A. G. A. Muthalif, Z. Zakaria, H. N. Shasmin, and S. C. Ng, "In-socket sensory system for transfemoral amputees using piezoelectric sensors: An efficacy study," *IEEE/ASME Trans. Mechatronics*, vol. 21, no. 5, pp. 2466–2476, Oct. 2016.

[20] A. Murgia, V. Kerkhofs, H. Savelberg, and K. Meijer, "A portable device for the clinical assessment of upper limb motion and muscle synergies," in *Proc. IEEE Eng. Med. Biol.*, Jan. 2010, pp. 931–934.

[21] O. A. Malik, S. M. N. A. Senanayake, and D. Zaheer, "A multisensor integration-based complementary tool for monitoring recovery progress of anterior cruciate ligament-reconstructed subjects," *IEEE/ASME Trans. Mechatronics*, vol. 20, no. 5, pp. 2328–2339, Oct. 2015.

[22] H. Ghasemzadeh, R. Jafari, and B. Prabhakaran, "A body sensor network with electromyogram and inertial sensors: Multimodal interpretation of muscular activities," *IEEE Trans. Inf. Technol. Biomed.*, vol. 14, no. 2, pp. 198–206, Mar. 2010.

[23] A. O. Posatskiy and T. Chau, "Design and evaluation of a novel microphone-based mechanomyography sensor with cylindrical and conical acoustic chambers," *Med. Eng. Phys.*, vol. 34, no. 8, pp. 1184–1190, Jan. 2012.

[24] C. Orizio, "Muscle sound: Bases for the introduction of a mechanmyographic signal in muscle studies," *Critical Rev. Biomed. Eng.*, vol. 21, no. 3, pp. 201–243, 1993.

[25] C. Orizio *et al.*, "Spectral analysis of muscular sound during isometric contraction of biceps brachii," *J. Appl. Physiol.*, vol. 68, no. 2, pp. 508–512, 1990.

[26] G. Oster and J. S. Jaffe, "Low frequency sounds from sustained contraction of human skeletal muscle," *Biophys. J.*, vol. 30, no. 1, pp. 119–127, Apr. 1980.

[27] R. Woodward, S. Shefelbine, and R. Vaidyanathan, "Pervasive motion tracking and muscle activity monitor," in *Proc. 2014 IEEE 27th Int. Symp. Comput.-Based Med. Syst.*, New York, NY, USA, 2014, pp. 421–426.

[28] K. T. Ebersole *et al.*, "MMG and EMG responses of the superficial quadriceps femoris muscles," *J. Electromyography Kinesiol.*, vol. 9, no. 3, pp. 219–227, Jun. 1999.

[29] A. K. Blangsted *et al.*, "Voluntary low-force contraction elicits prolonged low-frequency fatigue and changes in surface electromyography and mechanomyography," *J. Electromyography Kinesiol.*, vol. 15, no. 2, pp. 138–148, 2005.

[30] C. Orizio *et al.*, "The surface mechanomyogram as a tool to describe the influence of fatigue on biceps brachii motor unit activation strategy. Historical basis and novel evidence," *Eur. J. Appl. Physiol.*, vol. 90, no. 3–4, pp. 326–336, Oct. 2003.

[31] S. O. H. Madgwick, A. J. L. Harrison, and R. Vaidyanathan, "Estimation of IMU and MARG orientation using a gradient descent algorithm," in *Proc. IEEE Int. Conf. Rehabil. Robot.*, 2011, pp. 179–185.

[32] S. O. H. Madgwick *et al.*, "Measuring motion with kinematically redundant accelerometer arrays: Theory, simulation and implementation," *Mechatronics*, vol. 23, no. 5, pp. 518–529, Aug. 2013.

[33] X. Yun and E. R. Bachmann, "Design, implementation, and experimental results of a quaternion-based Kalman filter for human body motion tracking," *IEEE Trans. Robot.*, vol. 22, no. 6, pp. 1216–1227, Dec. 2006.

[34] J. Perry and J. Burnfield, *Gait Analysis: Normal and Pathological Function*, 2nd ed. Thorofare, NJ, USA: SLACK Inc., 2010.

[35] M. A. Islam, K. Sundaraj, R. B. Ahmad, N. U. Ahamed, and M. A. Ali, "Mechanomyography sensor development, related signal processing, and applications: A systematic review," *IEEE Sensors J.*, vol. 13, no. 7, pp. 2499–2516, Jul. 2013.

[36] C. Orizio *et al.*, "Surface mechanomyogram reflects muscle fibres twitches summation," *J. Biomech.*, vol. 29, no. 4, pp. 475–481, 1996.

[37] Y. Yoshitake and T. Moritani, "The muscle sound properties of different muscle fiber types during voluntary and electrically induced contractions," *J. Electromyography Kinesiol.*, vol. 9, no. 3, pp. 209–217, Jun. 1999.
[38] F. Esposito, C. Orizio, and A. Veicsteinas, "Electromyogram and mechanomyogram changes in fresh and fatigued muscle during sustained contraction in men," *Eur. J. Appl. Physiol. Occupat. Physiol.*, vol. 78, no. 6, pp. 494–501, Nov. 1998.
[39] D. McAndrew, M. Gorelick, and J. Brown, "Muscles within muscles: A mechanomyographic analysis of muscle segment contractile properties within human gluteus maximus," *J. Musculoskeletal Res.*, vol. 10, no. 1, pp. 23–35, 2006.
[40] D. Barry, "Acoustic signals from frog skeletal muscle," *Biophys. J.*, vol. 51, no. 5, pp. 769–773, May 1987.
[41] A. O. Posatskiy and T. Chau, "The effects of motion artifact on mechanomyography: A comparative study of microphones and accelerometers," *J. Electromyography Kinesiol.*, vol. 22, no. 2, pp. 320–324, 2012.
[42] A. Makni, H. Fourati, and A. Y. Kibangou, "Energy-aware adaptive attitude estimation under external acceleration for pedestrian navigation," *IEEE/ASME Trans. Mechatronics*, vol. 21, no. 3, pp. 1366–1375, Jun. 2016.
[43] F. Aghili and C.-Y. Su, "Robust relative navigation by integration of ICP and adaptive Kalman filter using laser scanner and IMU," *IEEE/ASME Trans. Mechatronics*, vol. 21, no. 4, pp. 2015–2026, Aug. 2016.
[44] H. Zhou and H. Hu, "Inertial motion tracking of human arm movements in stroke rehabilitation," in *Proc. 2005 IEEE Int. Conf. Mechatronics Autom.*, 2005, vol. 3, pp. 1306–1311.
[45] H. Tan, A. M. Wilson, and J. Lowe, "Measurement of stride parameters using a wearable GPS and inertial measurement unit," *J. Biomech.*, vol. 41, no. 7, pp. 1398–1406, Jan. 2008.
[46] H. Zhou *et al.*, "Use of multiple wearable inertial sensors in upper limb motion tracking," *Med. Eng. Phys.*, vol. 30, no. 1, pp. 123–133, Jan. 2008.
[47] P. Geethanjali and K. K. Ray, "A low-cost real-time research platform for EMG pattern recognition-based prosthetic hand," *IEEE/ASME Trans. Mechatronics*, vol. 20, no. 4, pp. 1948–1955, Aug. 2015.
[48] L. Bao and S. S. Intille, "Activity recognition from user-annotated acceleration data," in *Pervasive Computing*. New York, NY, USA: Springer, 2004, pp. 1–17.
[49] N. Ravi *et al.*, "Activity recognition from accelerometer data," in *Proc. Assoc. Adv. Artif. Intell.*, 2005, pp. 1541–1546.
[50] C. Kirtley, M. W. Whittle, and R. J. Jefferson, "Influence of walking speed on gait parameters," *J. Biomed. Eng.*, vol. 7, no. 4, pp. 282–288, 1985.
[51] C. BenAbdelkader, R. Cutler, and L. Davis, "Stride and cadence as a biometric in automatic person identification and verification," in *Proc. 5th IEEE Int. Conf. Automat. Face Gesture Recognit.*, 2002, pp. 372–377.
[52] R. Vaidyanathan *et al.*, "Biomechanical activity monitoring," Patent PCT/GB2014/053276, May 5, 2014.

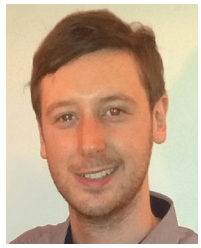

Richard B. Woodward (M'14) received the B.Sc. (Hons.) in cybernetics and control engineering from the University of Reading, Reading, Berkshire, U.K., in 2009, and the M.Sc. degree in biomedical engineering and neurotechnology and the Ph.D. degree in biomechatronics from Imperial College London, London, U.K., in 2011 and 2015, respectively.

He is a Postdoctoral Fellow with Northwestern University, Chicago, IL, USA, and also with Shirley Ryan AbilityLab, Chicago. His research interests include the fusion of human motion and muscle activity using wearable technology in order to gain greater insight into human ambulation outside of controlled environments, prosthetic technology, sensor design, and machine learning for advanced control of rehabilitation systems.

Sandra J. Shefelbine received the B.S.E. in mechanical and aerospace engineering from Princeton University, Princeton, NJ, USA, in 1997, the M.Phil. degree in engineering design from Cambridge University, Cambridge, Cambridgeshire, U.K., in 1998, and the Ph.D. degree in mechanical engineering from Stanford University, Stanford, CA, USA, in 2002.

She is an Associate Professor with the Department of Mechanical and Industrial Engineering, and also with the Department of Bioengineering, Northeastern University, Boston, MA, USA. Her work uses computational models, *in vivo* experiments, and clinical observation to understand musculoskeletal pathologies.

Ravi Vaidyanathan (M'08) received B.S., M.S., and Ph.D. degrees in mechanical engineering from Case Western Reserve University, Cleveland, OH, USA, in 1993, 1996, and 2001, respectively.

He is a Senior Lecturer of biomechatronics with Imperial College London, London, U.K. His current research focuses on mechanisms of sensory-motor control with an emphasis on biorobotics and human–robot interface.

Dr. Vaidyanathan is currently the Co-Chair of the IEEE Robotics and Automation Society Technical Advisory Committee on Biorobotics.